showed that one hidden layer resulted in the same performance as two or more hidden layers. Conflicting results were reported in the literature on the number of hidden nodes [18]. The selection of the number of hidden nodes in this study was purely based on the experiments. The selection of the EGG parameters was based on the statistical analysis of the EGG parameters between the patients with normal and delayed gastric emptying. Among the five parameters used as the input, statistical differences existed between the two groups of the patients in the percentages of the regular 2–4 cpm wave, the percentage of tachygastria, and the postprandial increase in EGG dominant power.

One may have noted that the accuracy of the method proposed in this paper for the prediction of gastric emptying is moderate and not very high. This is associated with the characteristic of gastric emptying and its association with gastric myoelectrical activity. Although the gastric motor function is usually the major player in gastric emptying, any abnormalities in the pylorus, such as pyloric stenosis, or in the small bowel, such as intestinal pseudoobstruction could lead to delayed emptying of the stomach. It is well known that gastric myoelectrical activity is only associated with gastric motor function and has nothing to do with the pylorus and the small intestine. It is, therefore, expected that the accuracy of the proposed method would not be very high. Particularly, the sensitivity is lower and the specificity is higher. This is because normal gastric myoelectrical activity cannot always guarantee normal gastric emptying and abnormal gastric myoelectrical activity usually results in delayed gastric emptying.

In summary, the proposed ANN method provides an alternative for the prediction of gastric emptying. In comparison with the conventional scintigraphic method of gastric emptying, the proposed method is noninvasive, well received among physicians and patients, and more cost effective.

ACKNOWLEDGMENT

The authors would like to thank J. Liang for his technical assistance and L. Dunnaway for her assistance in the preparation of the manuscript.

REFERENCES

[1] A. J. P. M. Smout, E. J. van der Schee, and J. L. Grashuis, "What is measured in electrogastrography?," *Dig. Dis. Sci.*, vol. 25, pp. 179–187, 1980.

[2] B. O. Familoni, K. L. Bowes, Y. J. Kingma, and K. R. Cote, "Can transcutaneous recordings detect gastric electrical abnormalities?," *Gut*, vol. 32, pp. 141–146, 1991.

[3] J. Chen, B. D. Schirmer, and R. W. McCallum, "Serosal and cutaneous recordings of gastric myoelectrical activity in patients with gastroparesis," *Amer. J. Physiol.*, vol. 266, pp. G90–G98, 1994.

[4] J. D. Z. Chen, Z. Y. Lin, and R. W. McCallum, "Abnormal gastric myoelectrical activity and delayed gastric emptying in patients with symptoms suggestive of gastroparesis," *Dig. Dis. Sci.*, vol. 41, pp. 1538–1545, 1996.

[5] J. D. Z. Chen and R. W. McCallum, "EGG parameters and their clinical significance," in *Electrogastrography: Principles and Applications*. New York: Raven, 1994, pp. 45–73.

[6] J. Chen, "A computerized data analysis system for electrogastrogram," *Comput. Biol. Med.*, vol. 22, pp. 45–58, 1992.

[7] R. C. Eberhart and R. W. Dobbins, *Neural Network PC Tools*. San Diego, CA: Academic, 1990.

[8] *Handbook of Neural Computing Applications*, Academic, New York, 1990.

[9] M. F. Moller, "A scaled conjugate gradient algorithm for fast supervised learning," *Neural Networks*, vol. 6, pp. 525–533, 1993.

[10] M. F. Kelly *et al.*, "The application of neural networks to myoelectric signal analysis: A preliminary study," *IEEE Trans. Biomed. Eng.*, vol. 37, pp. 221–230, Mar. 1990.

[11] T. Pike and R. A. Mustart, "Automated recognition of corrupted arterial waveforms using neural network techniques," *Comput. Biol. Med.*, vol. 22, pp. 173–179, 1992.

[12] S. Srinivasan, R. E. Gander, and H. C. Wood, "A movement pattern generate model using artificial neural networks," *IEEE Trans. Biomed. Eng.*, vol. 39, pp. 716–722, July 1992.

[13] I. N. Bankman, V. G. Sigillito, R. A. Wise, and P. L. Smith, "Feature-based detection of the K-complex wave in the human electroencephalogram using neural networks," *IEEE Trans. Biomed. Eng.*, vol. 39, pp. 1305–1309, Dec. 1992.

[14] J. Liang, J. Y. Cheung, and J. D. Z. Chen, "Detection and elimination of motion artifacts in electrogastrogram using feature analysis and neural networks," *Ann. Biomed. Eng.*, vol. 25, pp. 850–857, 1997.

[15] J. D. Z. Chen, Z. Y. Lin, Q. Wu, and R. W. McCallum, "Non-invasive identification of gastric contractions from abdominal electrodes using back-propagation neural networks," *Med. Eng. Phys.*, vol. 17, pp. 219–225, 1995.

[16] Z. Y. Lin, J. Maris, L. Hermans, J. Vandewalle, and J. D. Z. Chen, "Classification of normal and abnormal electrogastrograms using multilayer feedforward neural networks," *Med., Biol. Eng., Comput.*, vol. 35, pp. 199–206, 1996.

[17] J. D. Villiers and E. Barnard, "Backpropagation neural nets with one and two hidden layers," *IEEE Trans. Neural Network*, vol. 4, pp. 136–141, Jan. 1992.

[18] J. M. Zurada, *Introduction to Artificial Network Systems*. St. Paul, MN: West, 1992.

A New Video-Synchronized Multichannel Biomedical Data Acquisition System

Shengke Zeng*, John R. Powers, and Hongwei Hsiao

***Abstract*—This data acquisition system records video frames onto a video tape, and simultaneously acquires biomedical data along with video time codes onto a computer hard disk to achieve a 30-min video-synchronized data recording with a summed data rate of 2.16 Mbit/s. A time-code-bridge-file created during acquisition matches each video frame-start with the corresponding index number of the acquired data. The mean synchronization accuracy of the system is 0.22 ms.**

***Index Terms*—Data acquisition, multichannel, time code, video frame-start, video synchronization.**

I. INTRODUCTION

Video-synchronized data acquisition is finding more applications in biomedical engineering research. Some of these applications require a video-synchronized data-acquisition system with multidata

Manuscript received November 30, 1998; revised November 9, 1999. Part of this work was presented at the 21st Annual International Conference of the IEEE Engineering in Medicine and Biology Society, Atlanta, GA, October 13–16, 1999; Session 9.7.2, Data Acquisition & Measurement II, "16-channel 500-Hz video-synchronized EMG data acquisition." *Asterisk indicates corresponding author*.

*S. Zeng is with the National Institute for Occupational Safety and Health, 1095 Willowdale Road, Morgantown, WV 26505 USA (e-mail: saz0@cdc.gov).

J. R. Powers and H. Hsiao are with the National Institute for Occupational Safety and Health, Morgantown, WV 26505 USA.

Publisher Item Identifier S 0018-9294(00)01779-1.

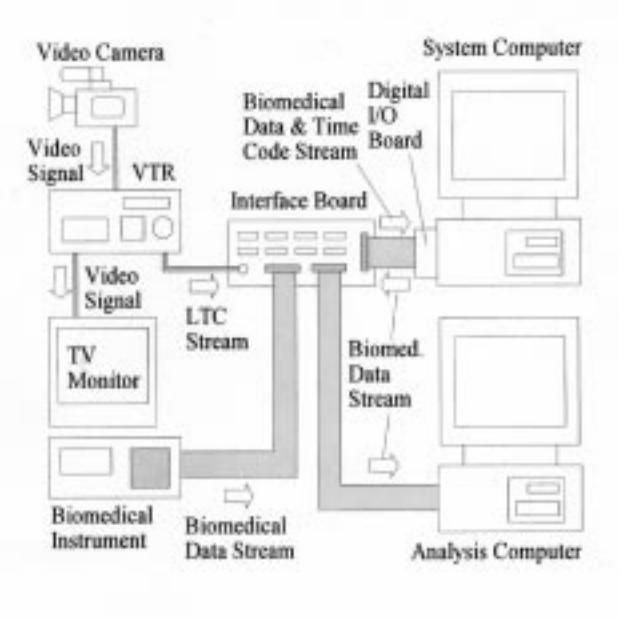

Fig. 1. System setup of the video-synchronized biomedical data acquisition system.

channels and high-frequency bandwidth, and also maintain long acquisition duration. One example of high-frequency application is frequency-domain muscle-fatigue analysis, for which a multichannel data acquisition system with a high raw-data signal frequency bandwidth of up to 3 kHz/channel is recommended [1]. A number of schemes have been published to achieve video-synchronized data acquisition [2]–[6]. Some of the schemes consist of simple event analyses stamped with video time codes [3], [6]. Some other sophisticated schemes have achieved multichannel data acquisition. Yen and Radwin utilized an audio-track digital recording method to record up to 32 channels of 8-bit data onto video tape audio tracks, and to record corresponding video images onto the video track of the same tape [4]. This method naturally synchronizes the video frames with the acquired data for extensive recording duration. But, because of the frequency-bandwidth limit of the audio tracks (20 Hz–20 kHz), the scanning frequency of the recorded data is limited to 60 Hz/channel. Higher-scanning-rate multichannel data acquisition was realized by using a high-speed video camera (1000 frames/s) which outputs a synchronization signal in each video frame to trigger a computer data acquisition sequence [5]. The maximum scanning frequency of this method may reach 1000 Hz/channel for 20 s of 1000 frames/s video recording. To acquire high frequency multichannel data for longer duration, Gaskill [6] suggested a data acquisition system using a digital audio tape recorder or a thermal chart recorder controlled by video time codes or vertical-video-sync pulses output from the video recording system.

This literature reports a new computerized data-acquisition system which extends Gaskill's suggestion by using a computer synchronization program to realize high-frequency long-duration video-synchronized biomedical-data acquisition. The system records the storage-intensive video images onto a video tape, and simultaneously acquires biomedical data and video time codes onto a computer hard disk. A time-code-bridge-file is created by the computer to synchronize the acquired biomedical data on the hard drive with the recorded human images on the video tape. Without manipulating video signals in the system computer, this separated recording method boosts the data acquisition speed, enables the realtime data synchronization and long

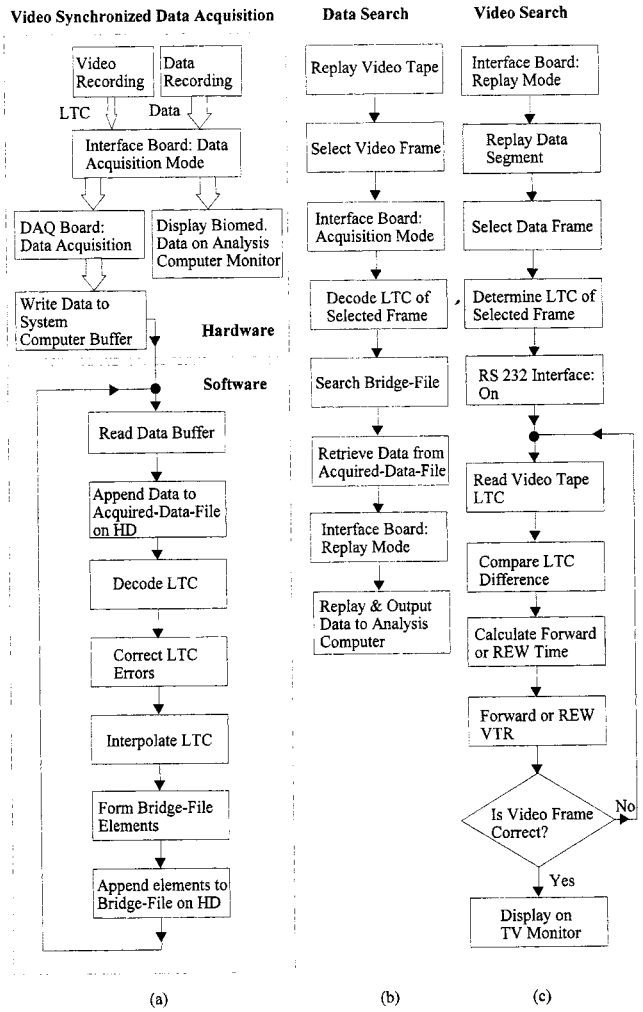

Fig. 2. Block diagrams of the data acquisition system.

recording duration. The video time-code frame-start bits were selected as the synchronization reference. With this reference, the synchronization error can be theoretically controlled within one Society of Motion Picture & Television Engineers (SMPTE) time-code bit duration (0.417 ms).

II. Method

As shown in Fig. 1, this computerized video-synchronized data acquisition system consists of a video camera to output NTSC color video signals, a digital video tape recorder (VTR) with a SMPTE longitudinal time code (LTC) output, a TV monitor, a multichannel biomedical-signal-measuring instrument with parallel digital output, a signal-interface board to condition the incoming and outgoing data and control the direction of data flow, a 266-MHz Pentium II microprocessor-based system computer with a 32-bit digital input–output (I/O) board, and an analysis computer if the system needs to run the instrument's own analysis software. LabVIEW graphical programming software (National Instruments, Austin, TX) was used to program the data acquisition, processing, storage and replay, and VTR control.

The system block diagrams are shown in Fig. 2. During video-synchronized data acquisition [Fig. 2(a)], the VTR records NTSC human activity images and outputs a 1-bit LTC stream to the interface board. The LTC stream is bi-phase modulated by frame numbers and sync

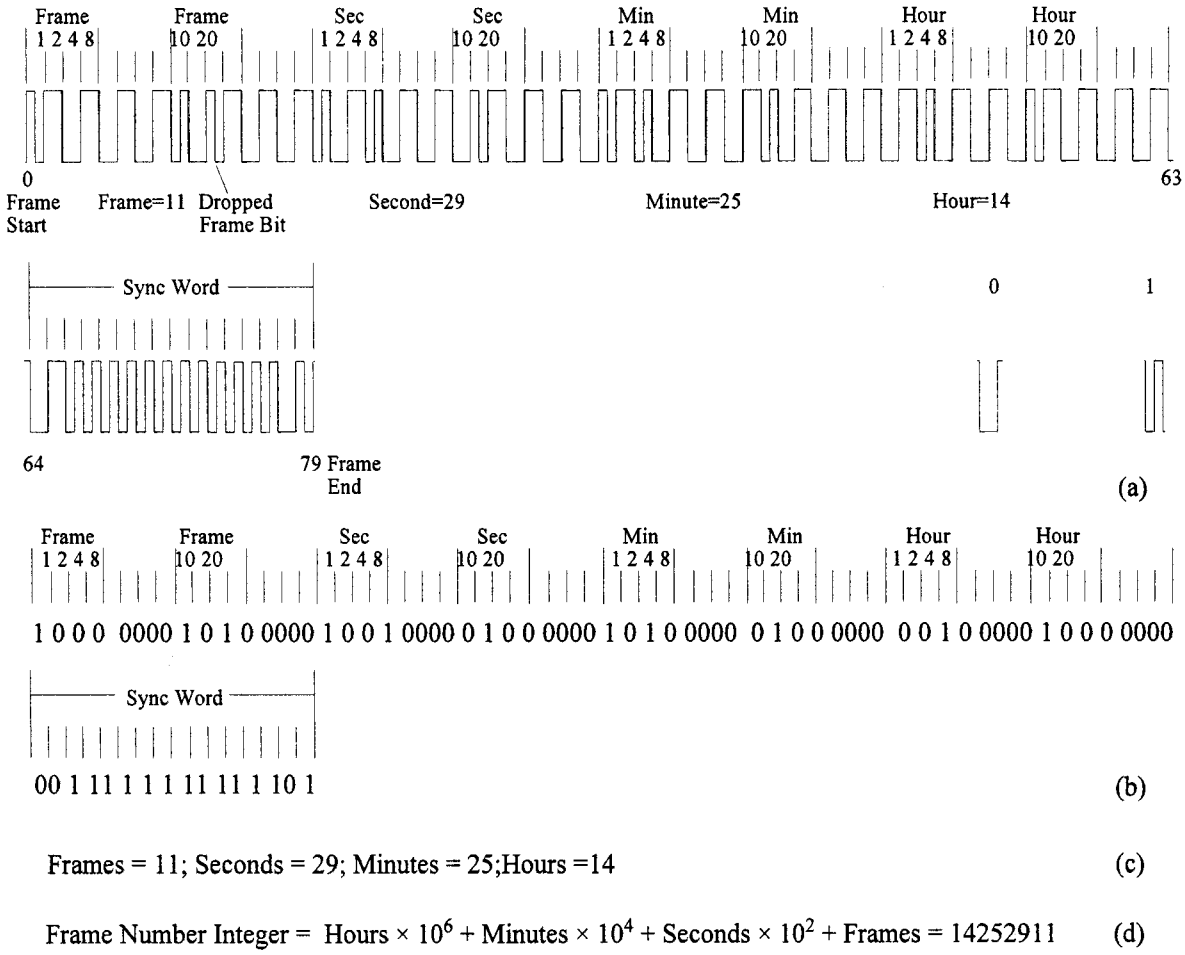

Fig. 3. SMPTE LTC decoding procedure.

words, as shown in Fig. 3(a) [7]. Simultaneously, the biomedical instrument measures human biomedical signals, and outputs up to 31 bits of data/sync signals to the interface board. The interface board in turn buffers the total of 32-bit data/sync/LTC signals, and outputs them to the 32-bit digital I/O board (National Instrument AT-DIO-32F). The interface board also directs the 31-bit data/sync signals to the data analysis computer for realtime data display. The digital I/O board scans the 32-bit signal stream at a scanning frequency of up to 72 kHz, converts the stream into 32-bit integers, and writes the integers into the system computer buffer. Whenever the buffer is half full, the program retrieves all the integers from the buffer, and appends them to an acquired-data-file on the hard disk [see Fig. 4(a) for acquired-data-file structure)]. In the meantime, the program retrieves the LTC bit stream from the integers, and sends the LTC stream to the decoding subroutine for LTC decoding. During decoding, the program determines the index number of the acquired-data-file at each video frame-start, and translates each 80-bit LTC into a unique eight-digit frame number integer as shown in Fig. 3(b)–(d). After decoding, the program forms a time-code-bridge-file with a two-column array. As shown in Fig. 4(b), the LTC column of the array contains the eight-digit frame-number integers of all recorded video frames, and the data-file-index column contains the corresponding index numbers of the acquired-data-file at frame-starts. In this way, each row of the array represents a unique video frame and its corresponding acquired-data-file index number at the frame-start. With this time-code-bridge-file, the computer is able to search for any data segment correspondent to a given video frame, or search for any video frame correspondent to a given data segment.

III. Hardware and Software Implementation

A. Interface Board

The main task of the interface board is to control the data flow direction. The interface board has two flow-control modes: data-acquisition mode and data-replay mode that are shown in Fig. 5(a) and (b), respectively. The flow-control mode is selected by the program which outputs a control bit from the digital I/O board to the interface board. The interface board buffers the incoming and outgoing data and converts the polarity of the LTC stream from 10 V to 0–5 V. In data-acquisition mode, the 31-bit data/sync signals from the biomedical instrument, and the corresponding 1-bit LTC stream from the VTR are input to the interface board. The interface board directs the total 32-bit data/sync/LTC signals to the data acquisition board for data acquisition, and directs the 31-bit data/sync signals to the data analysis computer for realtime display. In data-replay mode, the program outputs the desired 31-bit data/sync signal segment through the I/O board to the interface board. The interface board directs these 31-bit data only to the data analysis computer for further data analysis.

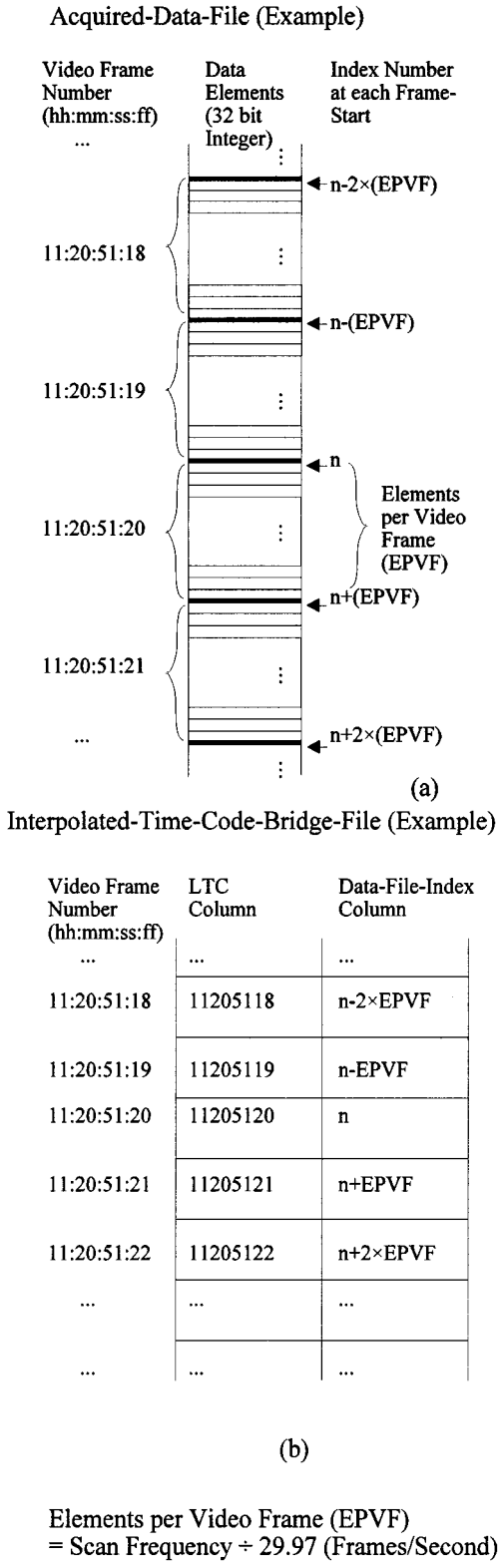

Fig. 4. Structure of the program files.

B. Acquired-Data-File

After every scan, the computer appends a 32-bit integer, which contains data/sync/LTC signals, as a file element to the acquired-data-file on the hard disk. As shown in Fig. 4(a), the acquired-data-file is a one-column array containing a large number of elements that equals the scanning frequency ×s of recording. Every video frame of the acquired-data-file contains a number of elements which equals scanning frequency 29.97 frames/s.

C. LTC Decoding Procedure

The SMPTE LTC output from the VTR are bi-phase modulated, as shown in Fig. 3(a). When the recorded signal pulse shifts up or down only at the extremes of the period for a signal bit (417 μs), the pulse is coded as a binary zero. A binary one is coded for a bit when a pulse shift occurs halfway through the bit period [7]. The first decoding step was to demodulate the bi-phase modulated LTC's to zeros and ones, as shown in Fig. 3(b). The second step is to determine the frame-starts. During decoding, the program continuously compares the demodulated 0-1 sequence with the 16-bit sync word pattern shown as the second row in Fig. 3(b). Whenever the pattern of any 16-bit segment of the 0-1 sequence matches that of the sync word, the bit after this segment would be determined as the frame-start bit. In the last step, the program converts 64 LTC bits from each frame-start bit into a unique eight-digit LTC integer, as shown in Fig. 3(c) and (d).

D. Interpolated Video Frame Decoding

During data acquisition, the program retrieves all 32-bit integers from the buffer whenever the buffer is half full, writes the data to the hard disk, decodes the LTC's and forms the time-code-bridge-file all in realtime. Even with a 266-MHz Pentium II microprocessor-based personal computer, the program cannot run fast enough for realtime decoding all LTC's (29.97 LTC's/s). The program decodes only one set of frame-start and LTC integer for every 15 video frames, and uniformly interpolates the remaining frame-start/LTC-integer values between current and last correctly decoded frame-starts. Since the video tape speed of a digital VTR is highly stable, the timing of the interpolated video frame-starts can be very accurate.

E. LTC Decoding Error Correction

LTC decoding errors can be caused by a VTR coding error, noise, electromagnetic interference and overflow of the computer buffer. The program has an LTC decoding error correction subroutine to detect decoding errors. The subroutine scrutinizes every decoded LTC to determine whether the decoded frame-start is within a predicted tolerance range (1/80 of a video frame, set by this program) and whether the decoded LTC integer matches the predicted number. If it is not, the program automatically discards this erroneous LTC.

F. Compact-Time-Code-Bridge-File and Interpolated-Time-Code-Bridge-File

After each LTC decoding, the program appends the correctly decoded frame-start and LTC integer to a compact-time-code-bridge-file. In turn, the program uniformly interpolates the frame-starts and LTC integers between the current and the last correctly decoded frame-starts, then appends the decoded and interpolated values to a two-column interpolated-time-code-bridge-file that contains the frame-starts and LTC integers of all recorded video frames (number of rows = 29.97 frames/s × seconds of recording), as shown in Fig. 4(b). Like the interpolated bridge file, the compact bridge file is also a two-column array except that it contains only decoded values. Its size is 1/15 of that of the interpolated bridge file when no decoding error occurs, and will be smaller if decoding errors occur and the consequent LTC decodings are discarded. When the program uses the bridge file for data segment or video frame search, it first searches the whole compact bridge file to determine an estimated file index number range, then searches only the portion of the interpolated bridge file within the estimated range to determine the exact index number of the acquired-data-file. This search

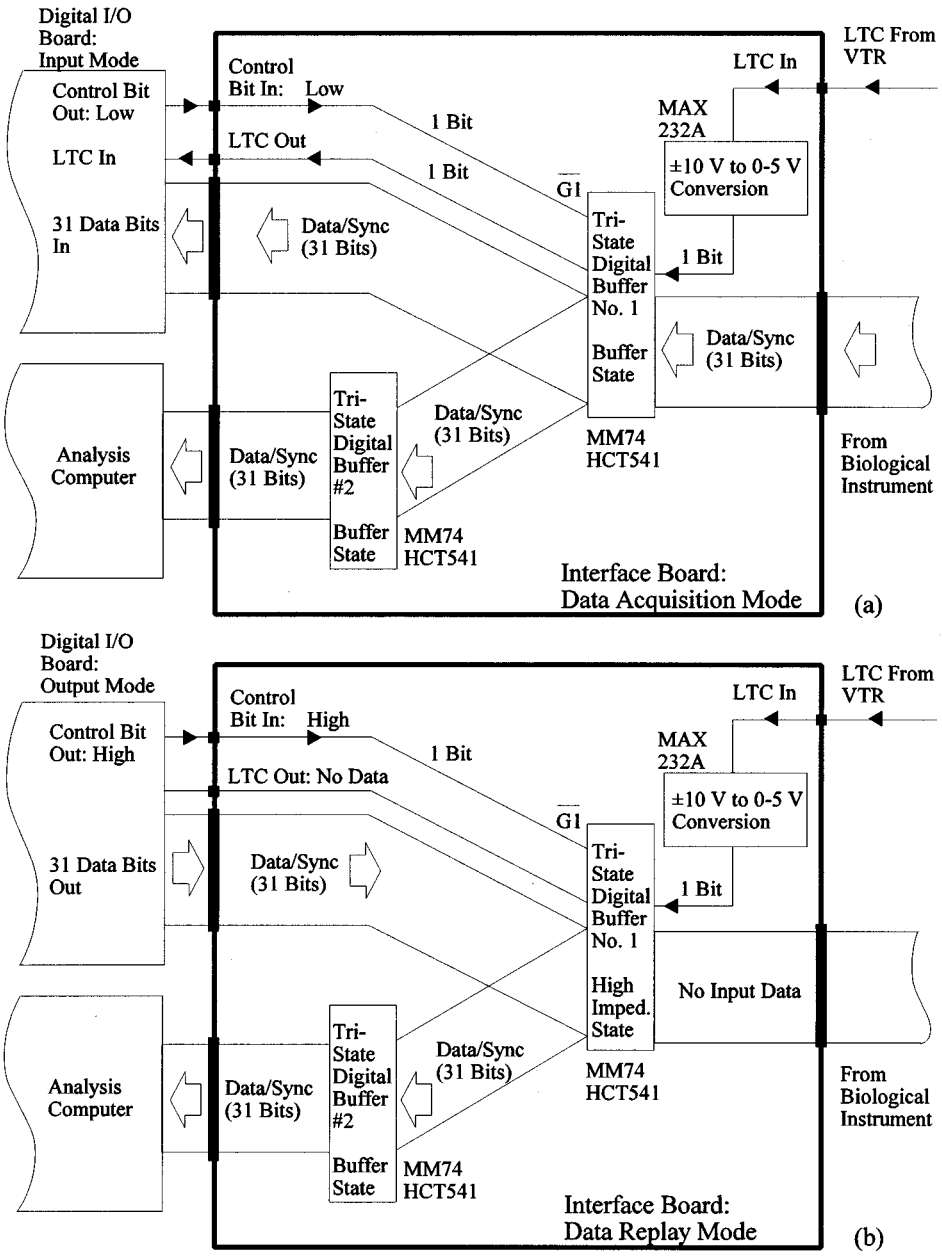

Fig. 5. Structure of the interface board.

procedure would reduce the data-searching time in long-duration data recording when the interpolated bridge file becomes very large.

G. Search for Data Segment

The flow chart for data search is shown in Fig. 2(b). When an interesting video frame is determined and frozen on the TV monitor during a video replay, the program turns the interface board to acquisition mode, acquires and decodes the frozen LTC. Then, the program searches the compact/interpolated time-code files for the corresponding frame-start index number of the acquired-data-file. Obtaining the expected corresponding index number, the program turns the interface board to the data-replay mode, retrieves the expected data segment from the acquired-data-file, displays it on the computer monitor and outputs it to the data analysis computer for further data analysis using the data analysis software.

H. Search for Video Frame

As shown in the video-search flow chart in Fig. 2(c), the interface board is switched to data-replay mode during video frame search. First, the program uses the compact/interpolated-time-code-bridge-files to retrieve a desired length of data from the acquired-data-file, replays the data frame-by-frame on the system and analysis computer monitors, and tracks the corresponding LTC's. When an interesting frame of replayed data is determined and frozen on the computer monitor, the program retrieves the corresponding LTC and controls the VTR through an RS232 serial bus to search for the expected video frame. First, the program reads the LTC of the current video-tape position through the RS232 interface and determines the difference between the video-tape LTC and the frozen-data LTC. Second, the program calculates the Forward or Rewind running time from the current video-tape position to the expected frame. The program then controls the VTR to forward or rewind the video tape to that frame. When the VTR stops, the program

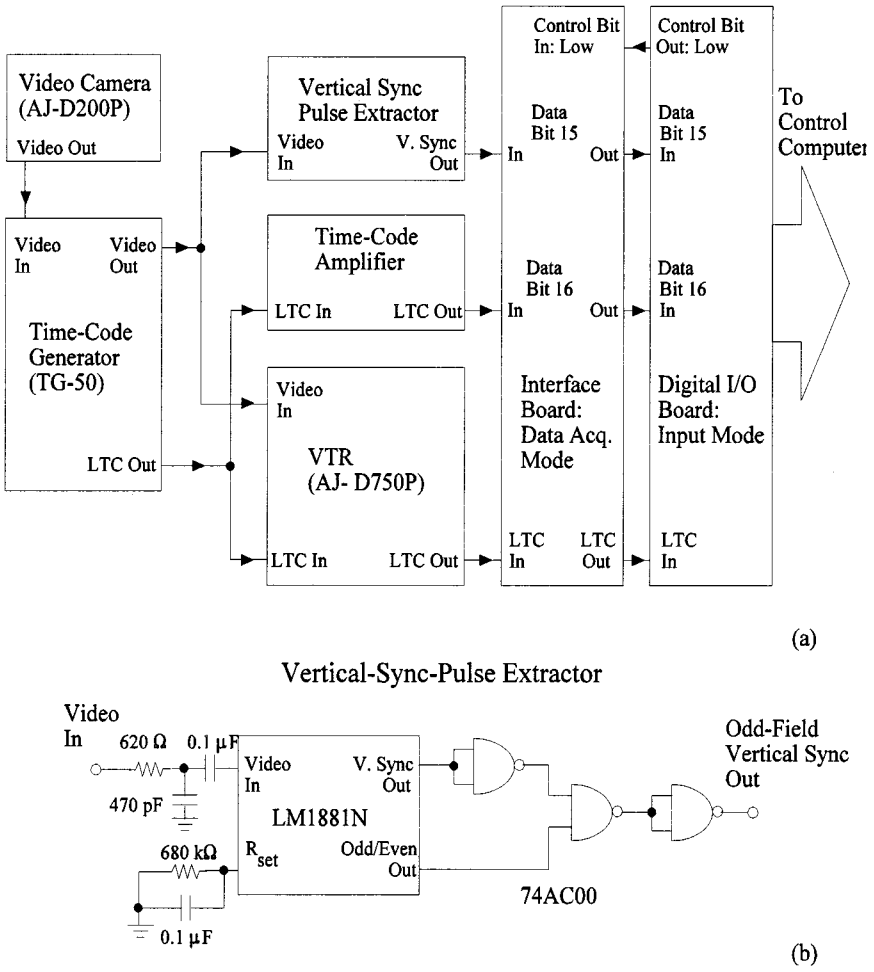

Fig. 6. Instrument setup for synchronization accuracy test.

finally examines the LTC from the VTR to determine whether the current LTC matches the expected frame number. If it is not, the program will repeat the search procedure.

IV. Synchronization Accuracy Test

In a synchronization accuracy test, an accuracy testing program compared the frame numbers, frame-starts and frame lengths of the acquired biomedical data with those of the recorded video time codes frame-by-frame, and calculated the mean and standard deviation of the whole acquisition synchronization errors. As shown in Fig. 6, the video vertical-sync pulses from a video camera (Panasonic AJ-D200P) and the corresponding LTC's were acquired by the system computer through the data channels as simulated dual-channel biomedical data. After data acquisition, the acquired LTC frame numbers of the simulated data would be compared with the corresponding frame numbers of the acquired LTC from the VTR to determine frame-number synchronization error; and the acquired vertical-sync pulses of the simulated data would be compared with the corresponding frame-starts of the acquired LTC from the VTR to determine synchronization errors in frame-start and frame length. This synchronization test was reliable because the two signal references, video vertical-sync pulses and the corresponding LTC frame-starts, are consistently synchronized.

In the test setup [Fig. 6(a)], the LTC was generated by an LTC generator (Horita TG-50) and synchronized with the video signals from a video camera (Panasonic AJ-D200P). The odd-field vertical-sync pulses were extracted from the video signals [Fig. 6(b)], and input to one of the 31data/sync channels (Bit 15) of the digital I/O board via the interface board as the simulated data for frame-start and frame-length comparisons. The LTC stream was input both to the data-channel Bit 16 via the time-code amplifier and interface board, and to the LTC In of

TABLE I
Comparison of Video-Synchronized Data Acquisition Systems

System	Bridge File	FSK Video [4]	Hi. Speed Camera [5]
Frame Rate (Frame/sec)	29.97	29.97	500
Type of Input Signal	Parallel	Serial	Un-specified
Summed Data Rate (kbit/sec)	2160	15.36	Un-specified
Number of Channels	30	32	2
Scanning Freq. / Channel (Hz)	6,000	60	500
Resolution (bit)	12	8	Un-specified
Max. Recording Duration (min)	30	≥120	0.33

TABLE II
COMPARISON OF THE SYSTEM SYNCHRONIZATION TESTS

System	Bridge File				FSK Video [4]
Replications	53835 (frames)				11848
Sync. Errors (mS)	Frame Number	Frame-start	Frame Length	Total	Total
Mean	0	-0.216	+0.003	0.219	16.6
Std. Dev.	0	0.124	0.062	0.186	0.1
Maximum	0	+0.653	+0.399	1.052	16.6
Minimum	0	0.000	+0.003	0.003	15.1

the I/O board via the VTR (Panasonic AJ-D750P) and interface board. The signal/data latencies through the VTR and interface board would be counted in the synchronization test.

After data acquisition, the accuracy testing program searched the bridge file for the acquired-data-file index at each frame-start, in order to retrieve the corresponding simulated data from the acquired-data-file. When the program obtained the simulated data, it first decoded the frame number of the acquired LTC from Bit 16, and determined the difference between the frame number of the LTC from Bit 16 and the frame number in the bridge file. Second, the program compared the timing difference between the rising edge of the odd-field vertical-sync pulse from Bit 15 and the corresponding frame-start in the bridge file. Finally, the program compared the duration difference between odd-field vertical-sync pulse period from Bit 15 and the corresponding frame-start period in the bridge file. The mean, standard deviation, and maximum and minimum values of these differences were then calculated.

V. RESULTS AND DISCUSSION

A. System Capacity

The use of the time-code-bridge-files enables this video-synchronized data acquisition system to perform data acquisition and subsequent video synchronization. The use of LTC decoding interpolation enables the system to perform the video synchronization with acquired data in realtime. Currently, the maximum scanning frequency for realtime video-synchronized 32-bit data acquisition (31-bit data/ sync signals, and 1-bit LTC stream) is 72 kHz without interruption. The maximum summed bit rate is 2.16 Mbits/s. This 32-bit data acquisition system can be flexibly configured. As the system is configured as a 30-channel-data plus one sync-signal channel with 12 bits of resolution, the maximum scanning frequency for each channel would be 6 kHz. At 72 kHz of the maximum scanning frequency, the maximum recording duration without data overflow is 30 min, which records 506.70 Mbytes of information onto the hard disk: 506.25 Mbytes for the acquired-data-file, 421.5 kbytes for the interpolated-time-code-bridge-file and 28.1 kbytes for the compact-time-code-bridge-file. The program effectively decoded the LTC stream in realtime with typically two decoding errors in 30 min of acquisition at 72 kHz. The decoding errors would be even fewer if a lower-scanning frequency were used in data acquisition. The program detects and discards all erroneously decoded LTC's to ensure that the two time-code-bridge-files are always error free. Table I shows a system comparison of this new method (bridge file based) with other published data.

B. Synchronization Accuracy

In the timing accuracy test, 1800 s of video signals and corresponding simulated-biomedical signals were acquired at a scanning frequency of 72 kHz using the testing setup in Fig. 6(a) and Fig. 6(b). The accuracy testing program examined the acquired-data-file and the interpolated-time-code-bridge-file, frame by frame. The frame numbers of the acquired video images and the corresponding simulated-biomedical data were examined to be totally synchronized without any detected frame-number errors. In the frame-start timing examination, the average frame-start of the recorded video images was slightly ahead of those of the simulated-biomedical data. In the frame-length examination, the average frame length of the recorded video images was slightly shorter than that of the simulated biomedical data. The mean total synchronization error ($|$frame-start error$|$ + $|$frame-length error$|$) was 0.219 ms (0.656% of a frame) and the maximum total synchronization error was 1.052 ms (3.153% of a frame). The maximum latency of the interface board (10.0 ns on rising edges and 18.0 ns on falling edges for biomedical data, and 1.24 μs on rising edges and 0.36 μs on falling edges for LTC's), was counted in the above synchronization errors. 166.80 ms of the VTR latency and 79.6 μs of the inherent phase difference between frame-starts and the odd-filed vertical-sync pulses were already compensated for in the accuracy testing program. The synchronization errors also counted in the timing errors caused by the VTR latency fluctuation, and by the vertical-sync pulse/frame-start phase difference fluctuation. The statistical test data of the new system along with other available synchronization-error test data (Yen/Radwin's FSK video-based system [4]) are listed in Table II for comparison.

This time-code-bridge-file method could also be applied to synchronize the biomedical data acquired on a computer hard disk and corresponding video frames acquired on the same or separate hard disk. The bridge file would be a three-column array, with a column of recorded video frame numbers, and two columns of the index numbers of the acquired video-signal file and data file, at the corresponding video frame-starts.

The weight of the interface board is less than 1 kg. Along with a laptop computer, a PCMCIA data acquisition card, and a compact VCR with LTC output, the whole system would be portable for field data collection.

VI. CONCLUSION

The system accurately synchronizes the acquired biomedical data recorded on the computer hard disk with the corresponding human activity images recorded on a video tape in realtime. With 2.16 Mbit/s of summed data rate and less than 1.1 ms of the maximum data-synchronization error, this data acquisition system is adequate for frequency-domain muscle-fatigue research, and would be a useful tool for human hazard exposure assessment, rehabilitation monitoring, and athlete monitoring in sport physiological programs.

REFERENCES

[1] D. G. Gerleman and T. M. Cook, "Instrumentation," in *Selected Topics in Surface Electromyography for Use in the Occupational Setting: Expert Perspectives*. Morgantown, WV: U.S. Department of Health and Human Services, Public Health Service, Centers for Disease Control, National Institute for Occupational Safety and Health, 1992, pp. 44–68.

[2] D. M. Gaskill, "Techniques for synchronizing thermal array chart recorders to video," in *Proc. 28th Int. Telemetering Conf.—ITC/USA/92*, vol. 28, 1992, pp. 61–64.

[3] M. Vannier *et al.*, "Time and motion studies of medical imaging workstations," *SPIE–Image Capture, Formatting, and Display*, vol. 1653, pp. 274–280, 1992.

[4] T. Y. Yen and R. G. Radwin, "A video-based system for acquiring biomechanical data synchronized with arbitrary events and activities," *IEEE Trans. Biomed. Eng.*, vol. 42, pp. 944–948, 1995.
[5] M. HGacía *et al.*, "Characterization of near-bed coherent structures in turbulent open channel flow using synchronized high-speed video and hot-film measurements," *Exp. Fluids*, vol. 19, pp. 16–28, 1995.
[6] T. Engström and P. Medbo, "Data collection and analysis of manual work using video recording and personal computer techniques," *Int. J. Ind. Ergonomics*, vol. 19, no. 197, pp. 291–298, 1997.
[7] D. M. Huber, *Audio Production Techniques for Video*. White Plains, NY: Knowledge Industry, 1987, pp. 93–100.

Multivariate Dynamic Analysis of Cerebral Blood Flow Regulation in Humans

Ronney B. Panerai*, David M. Simpson, Stephanie T. Deverson, Peter Mahony, Paul Hayes, and David H. Evans

***Abstract*—The contributions of beat-to-beat changes in mean arterial blood pressure (MABP) and breath-by-breath fluctuations in end-tidal CO_2 ($EtCO_2$) as determinants of the spontaneous variability of cerebral blood flow velocity (CBFV) were studied in 16 normal subjects at rest. The two input variables (MABP and $EtCO_2$) had significant cross-correlations with CBFV but not between them. Transfer functions were estimated as the multivariate least mean square finite impulse response causal filters. MABP showed a very significant effect in explaining CBFV variability ($p < 10^{-11}$, Fisher's aggregated-p test) and the model mean square error was significantly reduced ($p < 0.001$) by also including the contribution of $EtCO_2$. The estimated mean CBFV step response to MABP displayed the characteristic return to baseline caused by the cerebral autoregulatory response. The corresponding response to $EtCO_2$ showed a gradual rise taking approximately 10 s to reach a plateau of 2.5%/mmHg. This study demonstrated that spontaneous fluctuations in $EtCO_2$ can help to explain the CBFV variability at rest if appropriate signal processing techniques are employed to address the limited power and bandwith of the breath-by-breath $EtCO_2$ signal.**

***Index Terms*—Cerebral autoregulation, cerebral blood flow, cerebrovascular reactivity, cross-correlation analysis, Doppler measurements, end-tidal CO_2, system identification.**

I. Introduction

Two main mechanisms are responsible for controlling cerebral blood flow (CBF) under normal conditions. The first is cerebral pressure autoregulation which tends to maintain CBF relatively constant for changes in mean arterial blood pressure (MABP) in the interval from 50–170 mmHg [1]. Outside these limits cerebral autoregulation is said to be passive and CBF will follow changes in MABP [2]. The second major influence on CBF is the reactivity of cerebral vessels to arterial pCO_2. Hypercapnia leads to cerebral vasodilation and also reduces the efficiency of cerebral pressure autoregulation [2]–[4]. Conversely, hypocapnia is known to induce vasoconstriction and to widen the pressure range of cerebral pressure-autoregulation.

Both cerebral pressure-autoregulation and CO_2 cerebrovascular reactivity have been shown to be disturbed in pathophysiologic conditions [1], [2], [5]. These findings suggest that clinical tests for routine assessment of cerebral autoregulation and CO_2 reactivity might have potential clinical value for diagnosis and therapeutic management of patients with cerebrovascular disorders. Early attempts to quantify cerebral autoregulation adopted a static approach whereby relatively large changes in MABP were induced, usually by pharmacological methods. Corresponding changes in CBF were estimated from the mean value of long segments of data, in some cases reaching several minutes [1], [5]. The advent of Doppler ultrasound brought in the possibility of much higher temporal resolutions and has allowed studies of the dynamic response of autoregulation [4]. More recent work has shown that the autoregulatory dynamic response can be identified from spontaneous fluctuations in MABP and CBF velocity without the need to provoke large changes in these variables [6]–[11].

The most common technique to assess CO_2 reactivity is to measure changes in mean CBF (or flow velocity), as a consequence of breathing a mixture of 5% CO_2 in air [12]. Although most investigators use Doppler ultrasound to estimate the percent change in CBF from the change in CBF velocity (CBFV), the literature reflects little interest in the dynamic component of the CO_2-CBFV relationship. A number of physiological studies have shown that the CBF (or CBFV) response to a step change in CO_2 is not instantaneous but shows a relatively slow rise, lagging the CO_2 change by several seconds [13]–[15]. Poulin *et al.* [15] described the rising phase of CBFV by a simple exponential equation involving a time constant, an amplitude factor, and also a pure time delay of the order of 6 s. A more elaborate nonlinear model of CO_2 dynamics has been recently proposed by Ursino and Lodi [16] in which the interaction between cerebral autoregulation and CO_2 reactivity was also included through a sigmoidal relationship. The interaction between CO_2 reactivity and static autoregulation was also modeled by Czosnyka *et al.* [17] using representative characteristic curves implemented on a computer.

In the present study we explored spontaneous beat-to-beat fluctuations in MABP and breath-by-breath variability in end-tidal CO_2 ($EtCO_2$) in continuous recordings obtained from normal subjects at rest, to estimate the dynamic influences of arterial blood pressure and CO_2 on CBFV.

II. Methods

A. Patients and Measurements

The study was approved by the Leicestershire Research Ethics Committee, and informed consent was obtained from sixteen healthy volunteers between the ages of 23 and 51. Subjects were only included if they had no history of vascular disease, heart problems, hypertension, migraine, epilepsy, cerebral aneurysm, intra-cerebral bleeding or other neurological conditions.

All recordings were made with subjects in the supine position with the head elevated. Cerebral blood flow velocity (CBFV) was monitored in one middle cerebral artery (MCA) using a Scimed QVL-120 transcranial Doppler system in conjunction with a 2-MHz transducer held in position by an elastic headband. In accordance with a wide range of recent studies, CBFV was considered a suitable proxy for cerebral blood flow, as discussed in [4]–[7], [10], [15], and [22]. ABP was monitored noninvasively using a finger cuff device (Ohmeda 2300 Finapres

Manuscript received July 23, 1999; revised November 30, 1999. This work was supported in part by the Engineering and Physical Sciences Research Council (UK). *Asterisk indicates corresponding author.*

*R. B. Panerai is with the Division of Medical Physics, Faculty of Medicine, University of Leicester and the Department of Medical Physics, Leicester Royal Infirmary, Leicester LE1 5WW, U.K. (e-mail: rp9@le.ac.uk).

D. M. Simpson, S. T. Deverson, P. Mahony, and D. H. Evans are with the Division of Medical Physics, Faculty of Medicine, University of Leicester, Leicester Royal Infirmary, Leicester LE1 5WW, U.K.

P. Hayes is with the Department of Surgery, Leicester Royal Infirmary, Leicester LE1 5WW, U.K.

Publisher Item Identifier S 0018-9294(00)01778-X.